Synthesis and Self-Assembly of an Amphiphilic Poly(phenylene ethynylene) Ionomer†

Andrew P-Z. Clark, Ashley J. Cadby, Clifton Kwang-Fu Shen, Yves Rubin,* and Sarah H. Tolbert*

Department of Chemistry & Biochemistry, University of California Los Angeles, 607 Charles E Young Drive East, Los Angeles, California 90095-1569

Received: January 4, 2006; In Final Form: July 5, 2006

We have synthesized a conjugated amphiphilic polyelectrolyte, a poly(phenylene ethynylene) (PPE), and the structurally analogous neutral polymer. The solution-phase aggregation of the uncharged PPE can be reversibly controlled by varying the solvent polarity and concentration, while the charged polymer appears to self-assemble at any concentration in compatible solvents. These conclusions are based on a combination of absorption and photoluminescence spectroscopy and dynamic light scattering. Photoinduced absorption spectroscopy was also employed to investigate interchain electronic communication and the photoinduced production of free charge carriers. The uncharged PPE had a relatively high polaron yield, indicating π-stacking of adjacent PPE chains and efficient exciton splitting, while the charged polymer did not produce polarons, indicating that the polymers are not π-stacked despite their tendency to form aggregates. This is most likely due to the presence of the cationic trimethylammonium side chains which force neighboring polymer chains too far apart to achieve effective π-orbital overlap. Polarons were observed in both polymers after chemical doping with iodine. The ability to control aggregation and interchain electronic communication could be a useful tool in designing nanostructured electronic materials.

Introduction

Conjugated polymers have many potential applications in electronic and photonic materials as organic semiconductors.[1] They conduct electricity and are soluble in common solvents, facilitating processing by printing or thin film deposition and patterning. Recent research has led to functional devices of many types, including fluorescent sensors,[2,3] transistors,[4,5] LEDs,[6,7] lasers,[8,9] and photovoltaic cells.[10,11] Poly(phenylene ethynylene) (PPE) in particular could be useful for many of these applications, because it is a rigid rod polymer that is relatively stable in air. PPEs were initially studied for applications such as explosive detection,[12] molecular wires,[13] and polarizers for liquid crystalline displays.[14]

Like many conjugated polymers, PPEs have a tendency to form tertiary structures which can dramatically alter physical properties, depending on the type of structures formed.[15] To tune the electronic properties of PPE-based devices, the assembly of the polymer chains needs to be controlled. The conformation of the individual chains as well as the interactions between them strongly affect the optoelectronic properties of the system. This was demonstrated in the PPE system in an elegant study by Kim and Swager.[16] They synthesized several different PPE alternating copolymers consisting of various combinations of four different amphiphilic monomer units. These copolymers were deposited in Langmuir monolayers at an air−water interface, where the polarity of the side chains caused some polymers to adopt a conformation with all of the phenyl rings in the same plane (coplanar) and others to adopt a conformation with the phenyl ring on each repeat unit perpendicular to each of its nearest neighbors ("zipper" structure). By applying pressure to the films, some were found to switch reversibly between the zipper and the coplanar structures. The pressure-dependent transition from either of the coplanar structures to the zipper induced a substantial blue shift in the optical absorption. When all of the phenyl rings on a polymer chain are coplanar, the π system is fully delocalized, allowing access to the lowest energetic states. However, the conjugation can be interrupted by rotation of the phenyl rings, causing the persistence length of the excitons to decrease, thereby raising the energy of the accessible electronic transitions.

The structural conformations deduced from these data were also consistent with solution-phase spectroscopy. In solution, most PPEs appear to have a conformation similar to the zipper structure polymers in the Langmuir films. The conjugation of PPE molecules in solution is disrupted by rotation of the polymer backbone, which is facile in solution at room temperature due to the nearly cylindrical symmetry of the triple bonds.[17]

Aggregation of PPE chains, either in solution or in films, influences their photophysical properties by inducing planarization of the phenyl rings and by promoting interchain electronic communication through π-stacking. Solution-phase aggregation of PPE can be induced or inhibited by varying the solvent and concentration, which can effect both the chain conformation and interchain communication.[15] To achieve efficient packing and to avoid steric hindrance in aggregates, the solubilizing side chains on the phenyl rings must be aligned. This induces planarization of the PPE backbone, since all of the phenyl rings must be coplanar in order for the side chains to pack efficiently.[18] This allows for increased delocalization of the π-system, which is manifested as a discrete red shift in the optical absorption spectrum and the appearance of a two-state equilibrium between rotating and coplanar polymer chains. If the side chains are not too bulky, then neighboring polymer chains can π-stack, creating delocalized states with even lower

† Part of the special issue "Charles M. Knobler Festschrift".

* To whom correspondence should be addressed. E-mail: tolbert@chem.ucla.edu; rubin@chem.ucla.edu.

10.1021/jp060070d CCC: $33.50
Published on Web 08/11/2006

SCHEME 1: An Amphiphilic Poly(phenylene ethynylene) Ionomer

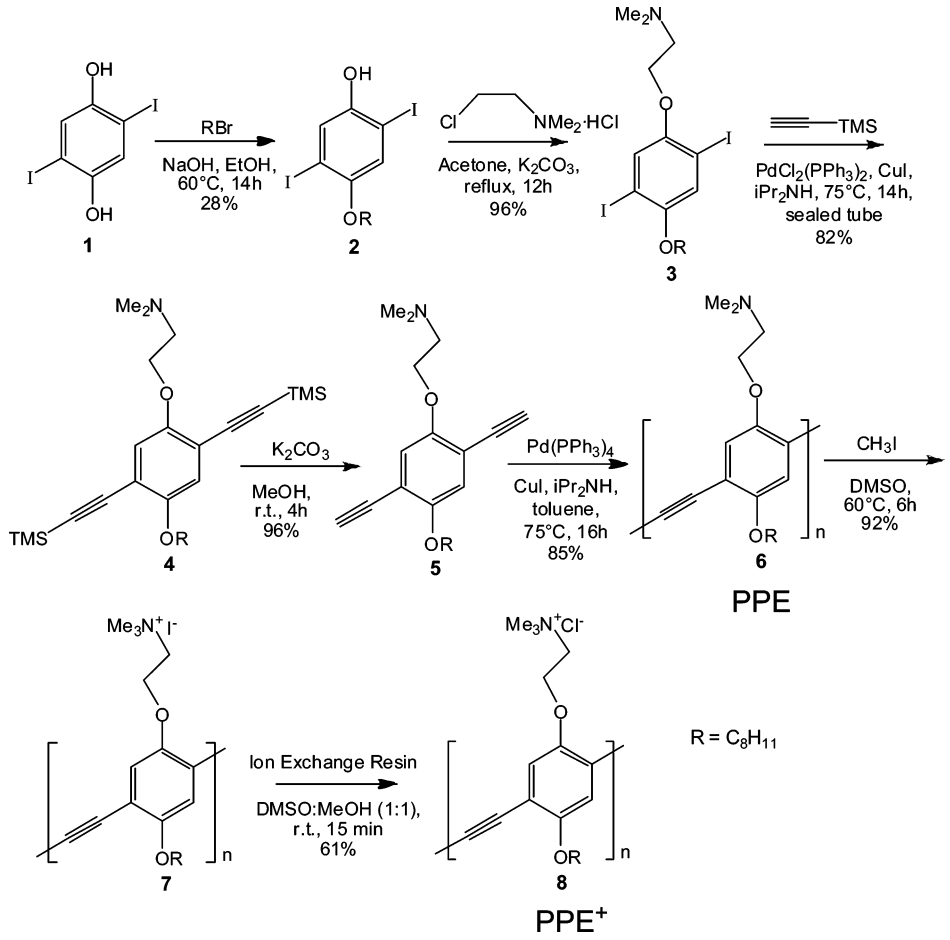

energy transitions. This can sometimes be observed as a narrow, red-shifted aggregate band in the absorption. This aggregation is often accompanied by decreases in luminescence quantum yield due to self-absorption and quenching.[19] As we will show here, the polymer conformation and the degree of aggregation can be controlled by choosing appropriate side chains and using the solvent and concentration to tune solution-phase chain aggregation. These changes can be observed simply through absorption and photoluminescence spectroscopy.

In this study, we have investigated an amphiphilic poly(phenylene ethynylene) ionomer (4-octyloxy-1-(2-trimethylammoniumethoxy)-2,5-poly(phenylene ethynylene) chloride) and the structurally analogous neutral polymer, whose structures are shown in Scheme 1. These polymers will henceforth be denoted by the abbreviations PPE^+ and PPE, respectively. The charged and uncharged polymers were both synthesized to compare the solution-phase self-assembly and its effects on polymer conformation and photophysics. Facially amphiphilic PPEs have been previously investigated,[16,19,20] but ionomeric PPEs have not been as widely studied.[21,22] In general, the solution-phase behavior of conjugated polyelectrolytes is influenced primarily by interchain and hydrophobic interactions, such as aggregation-induced conformational ordering and $\pi-\pi$ electronic communication.[23] Charged PPEs have a strong tendency to aggregate in solution, and like neutral PPEs, this aggregation induces planarization of the polymer backbones, which can be observed as red shifts in the optical absorption and emission.[22] In some polyelectrolytes, the degree of aggregation can be controlled by varying the pH.[24] However, the assembly of our PPE^+ is not pH sensitive, because there is no acidic hydrogen or electron pair on the quaternary trimethylammonium group.

Moreover, the rigid backbone of PPE^+ should discourage tight coiling, instead promoting formation of cylindrical micelles due to the amphiphilic nature of the side chains. Consisting of multiple, parallel straight-chain polymers, these micelles should act more like rigid rods. When incorporated into devices, it is hoped that these cylindrical micelles will function as wire-like structures, increasing carrier mobility over randomly coiled polymer aggregates.

Experimental Section

Polymer Synthesis. The synthesis of the amphiphilic PPE is fairly straightforward.[25] All reactions were performed under argon unless otherwise specified. 2,5-Diiodohydroquinone (**1**) can be monoalkylated in alkaline ethanolic solution to provide **2**.[26] Further derivatizing with 1-chloro-2-*N*,*N*-dimethylaminoethane gives **3** in excellent yield. Double Sonogashira couplings[27] add two acetylene moieties onto **3**, and the trimethylsilyl protecting group can be removed using K_2CO_3 in methanol, affording diyne **5**. Reaction of diiodo derivative **3** and diyne **5** with $Pd(PPh)_4$ as the catalyst provides polymer **6** in good yield, relatively high molecular weight (e.g., M_n = ca. 44 900, by gel permeation chromatography), and narrow polydispersity (ca. 1.27). Quarternization of PPE **6** with methyl iodide affords the charged PPE^+ **7** that is poorly soluble in water or methanol, possibly because of the regiorandom connectivities (e.g., head-to-head or head-to-tail) between adjacent phenyl rings.[28] However, exchanging the iodide counterion for chloride (**8**) increased water solubility by an order of magnitude.

Synthesis of 2,5-Diiodobenzene-1,4-diol (1). 2,5-Diiodo-1,4-dimethoxybenzene (22.0 g, 56.6 mmol) was dissolved in dichloromethane (150 mL) and cooled to −78 °C. A solution of boron tribromide (25 mL, 66.3 g) dissolved in dichloromethane (45 mL) was added dropwise. The resulting solution was warmed to room temperature while stirring overnight. The resulting reaction mixture was poured onto ice, and the solid was filtered and dried in vacuo to afford the pure product **1** (19.5 g, 53.9 mmol, 96%).

Synthesis of 4-Octyloxy-2,5-diiodophenol (2). Compound **1** (15 g, 41.4 mmol) was dissolved in a solution of sodium hydroxide (1.82 g, 45.5 mmol) in absolute ethanol (400 mL) at room temperature under Ar. The solution was warmed to 60 °C with constant stirring, followed by the dropwise addition of octyl bromide (7.15 mL, 41.4 mmol). After 18 h of stirring at 60 °C, the reaction mixture was cooled and filtered and the precipitate was washed with methanol. The filtrate was concentrated. The crude product was dissolved in a small amount of CH_2Cl_2 and purified by column chromatography (SiO_2; CH_2Cl_2/hexanes, 1:1 to 1:0) to yield the pure product **2** (5.5 g, 11.6 mmol, 28% yield).

Synthesis of [2-(4-Octyloxy-2,5-diiodophenoxy)ethyl]dimethylamine (3). A 250-mL round-bottom flask equipped with a magnetic stir bar was charged with anhydrous potassium carbonate (3.2 g, 23.1 mmol), 2-chlorotriethylamine hydrochloride (2.5 g, 17.3 mmol), and acetone (200 mL). The stirred mixture was purged with Ar for 30 min followed by the addition of 4-octyloxy-2,5-diiodophenol **2** (5.5 g, 11.6 mmol). After heating under reflux for 14 h, the reaction mixture was cooled and diluted with water (100 mL) to dissolve the salts. The product was extracted with ether and the combined organic phases were washed with 10% NaOH (aq), water, and brine. The solution was dried ($MgSO_4$) and filtered, and the solvent was evaporated to yield an oily solid. The crude product was purified by column chromatography (SiO_2; CH_2Cl_2/MeOH, 1:0 to 5:1) to yield the pure product **3** (6.1 g, 97%).

Synthesis of {2-[4-Octyloxy-2,5-bis(trimethylsilylethynyl)-phenoxy]ethyl}dimethylamine (4). A 50-mL sealed tube equipped with a magnetic stir bar was charged with [2-(4-octyloxy-2,5-diiodophenoxy)ethyl]dimethylamine **3** (4 g, 7.33 mmol), $(PPh_3)_2PdCl_2$ (257 mg, 0.37 mmol, 5 mol %), and CuI (100 mg, 1.32 mmol) under an Ar atmosphere. Diisopropylamine (10 mL) and toluene (10 mL) were added, and the clear solution was degassed by purging with Ar for 30 min. (Trimethylsilyl)acetylene (2.52 g, 3.11 mL, 25.7 mmol) dissolved in toluene (5 mL) was added by syringe into the vigorously stirring solution; a dark precipitate formed during the addition. Once the addition was complete, the reaction mixture was stirred at 75 °C for 18 h. After cooling, toluene (100 mL) was added. The resulting precipitate of ammonium iodide and palladium black was filtered off by passing the mixture through a plug of silica gel. Evaporation of the solvent gave a sticky, yellow oil. The crude oil was purified by chromatography (CH_2Cl_2/MeOH, 6:1) to yield the crude product **4** as a sticky oil, which was used directly in the next step without further purification.

Synthesis of [2-(4-Octyloxy-2,5-diethynylphenoxy)ethyl]-dimethylamine (5). Potassium carbonate (6.00 g, 43.4 mmol) was added under Ar to a solution of {2-[4-decyloxy-2,5-bis-(trimethylsilylethynyl)phenoxy]ethyl}dimethylamine **4** (complete sample from the previous step) in methanol (150 mL). The solution was stirred for 3 h before being poured into water. The aqueous layer was extracted with dichloromethane, and the organic extracts were washed with brine. The combined organic layers were dried with magnesium sulfate, and the solvent was removed by rotary evaporation. No further purification was necessary: the title compound **5** was afforded as a low-melting-point, light-yellow powder (1.8 g, 5.27 mmol; two steps, overall 71.8%).

Synthesis of Poly{[2-(4-octyloxy-2,5-diethynyl-phenoxy)-ethyl]dimethylamine} (6). A 100-mL Schlenk flask equipped with a stir bar was charged with [2-(4-octyloxy-2,5-diiodophenoxy)ethyl]dimethylamine **3** (890 mg, 1.63 mmol), {2-[4-octyloxy-2,5-bis(ethynyl)phenoxy]ethyl}dimethylamine **5** (500 mg, 1.46 mmol), and copper(I) iodide (18 mg, 0.1 mmol). The flask was purged and placed under a positive pressure of Ar, and $Pd(PPh_3)_4$ (56.6 mg, 0.05 mmol, 3 mol %) was added. The reaction mixture was further evacuated for 15 min and then purged with Ar. This procedure was repeated three times. Diisopropylamine (5.3 mL, 37.8 mmol) and toluene (15 mL) were added successively by syringe and then the mixture was immediately degassed by three freeze−pump−thaw cycles. The yellow fluorescent solution was warmed to room temperature over 10 min with vigorous stirring. The reaction mixture was heated to 80 °C while stirring for 20 h and then cooled to room temperature. The polymer was precipitated by pouring the dark-reddish reaction mixture into acetone (150 mL). The polymer was collected by centrifugation, washed with CH_3CN, and then redissolved in benzene. The resulting polymer was collected by evaporating the benzene and then washing the residue with THF and dichloromethane to give polymer **6** as a dark-orange film (200 mg, 39%).

Synthesis of Poly{[2-(4-octyloxy-2,5-diethynylphenoxy)-ethyl]trimethylammonium iodide} (7) and Poly{[2-(4-octyl-oxy-2,5-diethynylphenoxy)ethyl]trimethylammonium chloride (8). A 50-mL sealed tube equipped with a magnetic stir bar was charged with polymer **6** (200 mg), iodomethane (4.0 mL), and DMSO (10 mL). The contents were stirred at 60 °C for 16 h. During this time, gel formation occurred. The quaternarized polymer **7** was precipitated as its iodide salt by pouring the mixture into acetone (300 mL). The precipitate was allowed to settle and then the majority of the liquid was decanted off. The solid was washed with ether, collected by centrifugation, and dried under vacuum overnight. The polymeric iodide salt (261 mg, 90%) was subjected directly to a mixture of anionic ion-exchange resin (1 g, Fischer Rexyn 202, presaturated with 0.1 M aqueous NaCl), DMSO (5 mL), and MeOH (3 mL). After stirring for 10 min, the mixture was filtered and transferred into a 500-mL Erlenmeyer flask. An acetone/ether mixture (2:1, 300 mL) was added to the flask, which resulted in precipitation of the polymer. After settling, most of the solvent was decanted off. The polymer was collected by centrifugation and dried under vacuum overnight to yield **8** as a yellow powder (198 mg, 95%).

Analysis. All NMR spectroscopy studies were carried out using Bruker AMX-500, Avance-500, AMX-400, or Avance-600 spectrometers. Tetramethylsilane (TMS) or residual protonated solvent ($CDCl_3$, $C_2D_2Cl_4$, or d_6-DMSO) was used as the internal standard for ^{1}H NMR spectra, and the deuterated solvent ($CDCl_3$ or $C_2D_2Cl_4$) was used as a standard for ^{13}C NMR spectra. High-resolution electron−ionization mass spectra (HRMS) were obtained using a VG Autospec EI/CI double-focus magnet mass spectrometer. High-resolution matrix-assisted laser desorption ionization time-of-flight (MALDI-TOF) mass spectra were obtained using an Applied Biosystem DE-STR MALDI-TOF mass spectrometer or an IonSpec Ultima 7T MALDI FT mass spectrometer. The matrix used for the MALDI-TOF/FT MS was α-cyano-4-hydroxycinnamic acid, dihydroxbenzoic

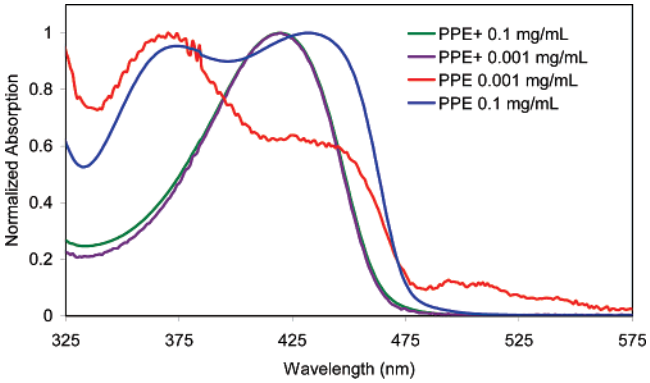

Figure 1. Absorption spectra of charged and uncharged PPE at high and low concentration. PPE^+ in ethanol shows only the aggregated, planar conformation. PPE in THF shows two peaks which scale with concentration, corresponding to the planar conformation and an isolated, freely rotating conformation.

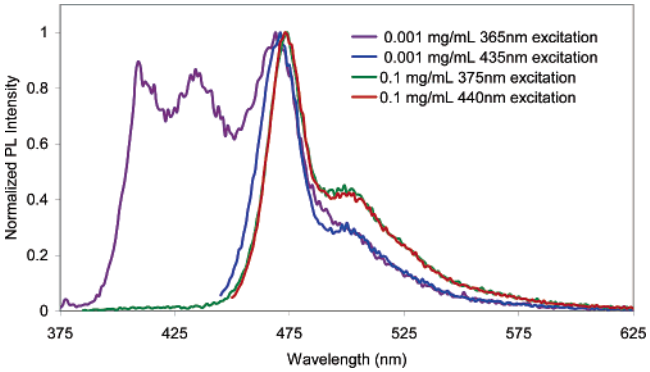

Figure 2. Photoluminescence spectra of uncharged PPE in THF, showing emission only from a planar state at high concentration, regardless of the excitation energy. When the polymer is diluted so that more unaggregated polymer is present, excitation at bluer wavelengths can produce blue-shifted emission which originates from nonaggregated polymer chains with freely rotating phenyl rings.

acid, or terthiophene. Fourier transform infrared (FTIR) spectra were recorded on a Perkin-Elmer Paragon-1000 instrument. Flash column chromatography was performed on silica gel 230-400 mesh from E. Merck or from Scientific Absorbents; thin-layer chromatography (TLC) was performed on glass plates coated with silica gel $^{60}F_{254}$ from E. Merck.

All solution-phase photophysics and light scattering measurements were carried out on samples made by dissolving solid polymer samples in the appropriate solvent. Solvents used for light scattering were filtered at least 3 times using 0.2 μm syringe filters. The samples were then transferred to 10 mm path length, 4 mL quartz cuvettes for measurement. UV−vis absorption measurements were conducted on a Perkin-Elmer Lambda 25 spectrometer. Photoluminescence (PL) measurements were carried out using a Jobin Yvon Horiba Fluorolog-3 spectrofluorometer. Photoinduced absorption (PA) measurements were recorded on a custom-built spectrometer. Samples were excited with either a Spectra-Physics Series 2000 Ar^+ laser emitting at 457 or 488 nm or a JDS Uniphase model NV-10210-100 tripled YAG operating at 355 nm; all lasers were chopped using a Stanford Research Systems optical chopper. Samples were illuminated with a tungsten lamp, and the transmitted light was collected by a CVI Spectral Products 1/4 M Digikrom monochromator with a silicon diode detector. A Stanford Research Systems Model SR810 lock-in amplifier was used to record the resulting change in transmission. Light scattering measurements were recorded with a Beckman Coulter N4 Plus submicron particle size analyzer.

Results and Discussion

Several different techniques were employed to elucidate the aggregation behavior of the charged and uncharged polymers and its effects on their optical properties. UV−vis absorption spectra of both polymers at different concentrations are presented in Figure 1. In good solvents such as tetrahydrofuran (THF), PPE displays two distinct absorption peaks whose relative intensities scale with concentration. The high-energy peak centered at 375 nm corresponds to a randomly oriented, freely rotating, or "twisted" conformation which is blue shifted due to the interruption in conjugation caused by incomplete overlap of the π-orbitals between phenyl rings on adjacent repeat units, thereby widening the band gap. This peak is increased in relative intensity at low concentration because more of the polymers are isolated in solution, where the phenyl rings are free to rotate. The peak centered at 435 nm corresponds to an aggregated, planarized conformation, in agreement with previous studies on dialkoxy-substituted PPEs.[29] At high concentration, more of the chains are incorporated into aggregated domains, increasing the relative intensity of this planar peak.

PPE^+ is soluble in polar solvents such as ethanol and water. As shown in Figure 1, it displays one absorption peak in ethanol with a maximum at 420 nm, corresponding to the planar conformation. It forms aggregates at any concentration with measurable optical density because of the affinity of the trimethylammonium groups for the polar solvent and the insolubility of the octyloxy side chains. Like surfactants, the polymers likely form micelles, exposing the charged groups to the solvent and isolating the alkoxy groups in the center of the domains. To achieve efficient packing of the side chains in the micelles, the polymers must pack in a regular arrangement, forcing them to adopt the planar conformation. The PPE^+ absorption transition at 420 nm arises from polymers which probably have a similar backbone conformation as the planar uncharged polymer but the absorption maximum is blue shifted by 15 nm in PPE^+ compared to PPE. There are several possible causes for this shift, including the change in dielectric constant of the surrounding environment (solvatochromism) due to the more polar solvent and the presence of charged groups. The cationic side chains could also induce a slight deviation in the dihedral angle between neighboring phenyl rings due to electrostatic repulsion. This would lead to incomplete delocalization of the π-system and contribute to the blue shift in absorption. Repulsion of the cationic side chains could be another possible cause for this shift. Finally, since PPE does not have charged side chains, it might be able to achieve some degree of electronic interaction between adjacent polymer chains. Although it does not display the sharp, red-shifted absorption peak characteristic of π-stacked aggregates,[19] a small degree of π-overlap could contribute to the red-shifted absorption of PPE compared to PPE^+.

Photoluminescence spectra of both polymers, shown in Figures 2 and 3, support the conformational models proposed above. These spectra were recorded on the same solutions as the UV−vis spectra in Figure 1, at two different excitation energies, corresponding to the two peaks in the absorption spectra. If any sample is excited at 420 nm, emission is always from the low-energy coplanar conformation with a peak around 470 nm. Excitation of PPE^+ at 375 nm yields only 470 nm emission (Figure 3), indicating that all of the polymers are in the planar conformation, as suggested by the UV−vis spectra. When the uncharged polymer is excited at 375 nm, the concentrated sample emits only from the coplanar conformation,

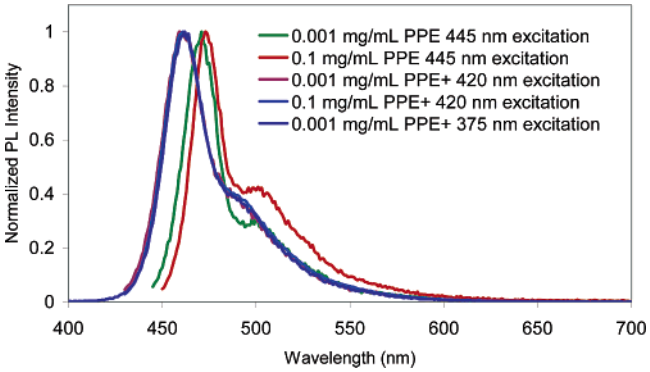

Figure 3. Photoluminescence spectra of PPE^+ in ethanol and PPE in THF. Regardless of the excitation energy or the polymer concentration, PPE^+ always shows an emission peak near 470 nm, indicative of the planar chain conformation. Comparison of planar PPE with the PPE^+, however, indicates that the luminescence is slightly blue shifted in the PPE^+ compared to the PPE, probably due to increased interchain interactions in PPE or some small degree of twisting in the PPE^+.

whereas the dilute sample shows additional peaks at 410 and 430 nm. This suggests that the majority of the polymer chains are aggregated or within a Förster radius of aggregated polymer at high concentration, allowing them to absorb at 375 nm but emit only at 470 nm after energy transfer to a lower energy planar state. At low concentration, there are also some isolated chains, which absorb at 375 nm and emit from the twisted state at 410 nm, with the corresponding vibronic band at 430 nm. There are also some aggregated chains that can emit at 470 nm.

In Figure 3, there is a shift of approximately 12 nm between the peak emission of the charged and uncharged polymers. Like the shift in absorption peaks between PPE and PPE^+, PPE has a lower energy emission, likely due to solvatochromism, to electrostatic repulsion causing a slight backbone twist, and/or to increased π-orbital overlap between aggregated chains in PPE relative to PPE^+. If π-overlap contributes to this shift, one might expect to observe fluorescence from excimer-like complexes. Excimer fluorescence has been observed in PPE as the characteristic broad, strongly red-shifted peak in the PL spectrum.[22] In agreement with this hypothesis, Figures 2 and 3 both reveal an increased intensity in the low-energy tail in concentrated samples of uncharged PPE, which is not observed in dilute PPE or any concentration of PPE^+.

To help further distinguish between solvatochromic effects and changes in π-orbital overlap, it is useful to perform an experiment that is extremely sensitive to π-orbital interactions. One such experiment is the photogeneration of free charge carriers. Since this polymer is designed to be used in nanostructured electronic devices, it is also useful to know if free charge carriers can be photogenerated efficiently. Previous work on other semiconducting polymers, such as poly(phenylene vinylene) (PPV), has shown that polarons are the dominant charge carriers.[30,31] Our group has investigated the photoinduced charge carrier production in poly[2-methoxy-5-(2′-ethylhexyloxy)-1,4-phenylene vinylene] (MEH-PPV), finding that photoinduced charge carrier production is sensitive to interactions between neighboring polymer chains.[32] By incorporating MEH-PPV into the pores of mesoporous silica with various pore sizes, we were able to vary the number of polymer chains in each pore, from single chains (small pores with ~2 nm diameter), to small aggregates of parallel straight chains (medium pores ~5 nm), to larger aggregates of coiled chains (large pores ~8 nm). Using photoinduced absorption (PA), we found that the polaron yield was low in the small pore samples but it increased dramatically in the medium and large pores.[32] This trend was

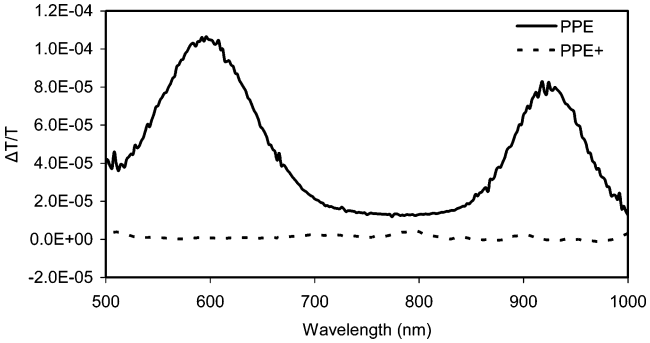

Figure 4. Photoinduced absorption spectra (RMS) of PPE^+ in ethanol and PPE in THF, showing polaron and triplet absorption in the uncharged PPE, but no signal in charged PPE^+, likely due to the lack of π-overlap.

attributed to the varying polymer conformations and particularly to the different degrees of interchain interaction. For polarons to form efficiently, the excitons must split, remaining separated and unable to recombine on the relatively slow time scale of the PA experiment. The data suggested that formation of an interchain exciton (with one carrier on each chain) was necessary for efficient polaron production.[32] Formation of such an interchain exciton, in turn, requires good π-stacking between neighboring chains.

This generalization is of paramount importance in the design of electronic materials. For example, a system which can produce photoinduced free charge carriers and prevent them from recombining rapidly is ideal for a photovoltaic cell, but it would make a poor light emitting device (LED). Conversely, limiting the polaron yield and maximizing carrier recombination would lead to high-quality LEDs but poor solar cells. The absorption and photoluminescence data above suggests that we have two such systems: PPE, which can form π-stacked aggregates in solution, and PPE^+, which forms noninteracting aggregates. We will now look at photoinduced absorption to evaluate this model.

The PA spectrum of PPV is dominated by a broad polaron signal between 600 and 1000 nm.[33] Polarons can recombine to form triplets, which are also evident in the PA spectrum with an absorption around 900 nm.[34] Polarons and triplets with similar energies to those of PPV have been previously observed in PA experiments on PPE.[35] In PPEs, a polaron peak is observed at 650 nm and a triplet peak is found at 855 nm. The polaron was only observed in a PPE with linear butyl side chains, whereas a PPE with branched ethylhexyl side chains showed no polaron signal. This indicates that interchain electronic communication, which is hindered by the bulky branched side chains, is necessary to observe a polaron in photoinduced absorption.

Photoinduced absorption of our polymers, presented in Figure 4, shows two peaks in agreement with previous studies discussed above. These two peaks, centered at 590 and 920 nm, can be assigned to a polaron and to a triplet, respectively. Both peaks are evident in PPE, but no signal is observed for the PPE^+ polyelectrolyte. The presence of these signals in PPE and their absence in PPE^+ supports the aggregation hypothesis presented above. The polaron separates the charges across different chains in the uncharged polymer, whereas the lack of effective π-overlap in PPE^+ prevents efficient interchain electronic communication. Therefore, if polarons are formed, they are likely confined to a single chain where they can recombine rapidly before they can be detected in the relatively slow PA experiment. The absence of the triplet signal also indicates that the polaron yield is very low, because triplets are

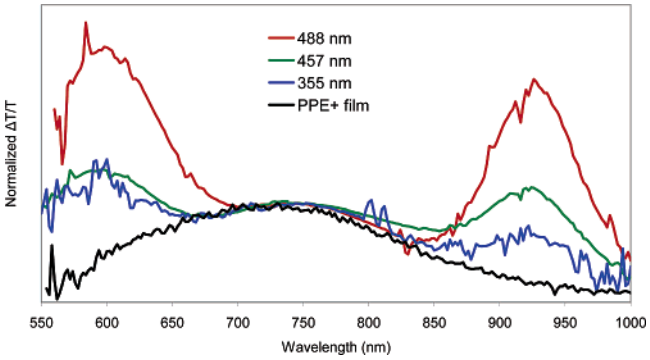

Figure 5. In addition to the polaron and triplet absorptions shown in Figure 4, a third peak centered at 730−750 nm is often observed in noninteracting PPE chains.[36] This peak is observed in PPE in THF at bluer excitation energies and in drop cast films of PPE^+ excited at 457 nm. While the exact spectroscopic assignment of this peak is not clear, it seems to be a long-lived excited state that appears when extra energy is put into the system or under conditions where exciton splitting to form polarons is not favored.

often formed by polaron−polaron fusion.[33] We note that there are small differences in the polaron and triplet energies observed in our materials and those reported previously in the literature.[35] This could be due to the difference in side chains between our dialkoxy substituted PPEs and the dialkyl PPEs reported in the literature. Specifically, because the triplet excitations are largely confined to the phenyl rings, the electron-donating oxygen atoms bound to the rings might be expected to lower the energy of the triplet when compared to the alkyl-substituted phenyl rings.

Further evidence for the lack of electronic communication between polymer chains in PPE^+ can be found in additional PA experiments. As shown in Figure 5, when the uncharged PPE is excited at higher energies (i.e., bluer wavelengths), a third peak is observed in the PA spectra, centered at ∼750 nm. While the exact assignment of this peak is not clear, it has been associated with highly noninteracting PPE chains. For example, a similar signal was previously observed in a PPE with extremely large, bulky, saturated polycyclic side chains.[36] If the PPE^+ is cast into a film, so that the chains are forced into slightly closer proximity, this same ∼750 nm peak is observed (Figure 5). The intensity of the peak steadily increases with decreasing temperature in the range between 30 and 240 K, consistent with an excited-state absorber. While there is some debate as to the exact nature of this excited-state species, it seems to be a long-lived excited state that appears when extra energy is added to the system or under conditions where exciton splitting to form polarons is not favored (i.e., when PPE chains are isolated).

As demonstrated by the PA experiments, charge carriers can be generated optically in solution in the uncharged PPE but not in PPE^+ because of the lack of π-overlap. In an effort to further characterize the potential for producing charge carriers, we doped the polymers, which can generate charges chemically. Iodine was added to a solution of each polymer, abstracting an electron to form I_3^- and *p*-doped polymers. Absorption spectra of both doped polymers, normalized and corrected for the iodine absorption, are shown in Figure 6. The polaron is evident in both polymers, but the signal is much weaker (before normalization) in the charged polymer. This could be due to the presence of the cationic side chain, which in proximity to the doped polymer would likely destabilize the *p*-polaron. In addition, there is no triplet signal as in the photoinduced absorption. This supports the accepted mechanism of triplet production[33] in the photoexcited samples (polaron−polaron fusion), because in doped samples the only charge carriers are

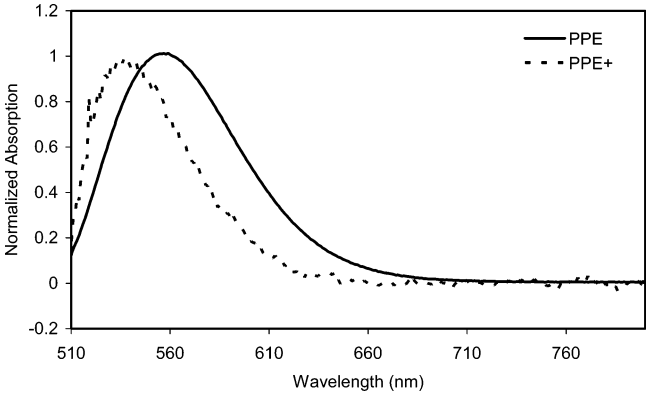

Figure 6. Absorption of PPE in THF and PPE^+ in ethanol, both doped with iodine. Polaron absorption is evident, but unlike the photoinduced absorption, no triplet signal is observed because there is only *p*-doping. The signal from the uncharged PPE is stronger and red shifted, likely because the polaron is more delocalized than in PPE^+ and because the cationic side chain destabilizes the *p*-polaron in PPE^+.

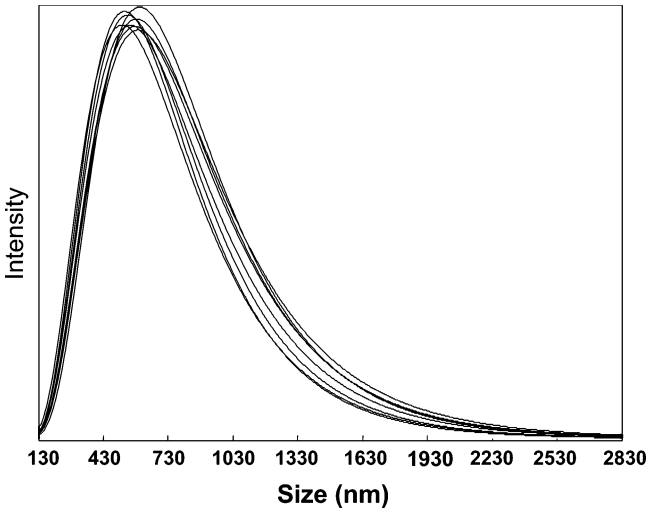

Figure 7. Unimodal light scattering data for uncharged PPE showing reproducibility and average size ∼600 nm. Multimodal analysis shows the presence of a large number of smaller scatters <100 nm as well. These likely correspond to single polymer chains. The multimode fits contain more variables, however, and thus are not as robust. As a result, they show significantly more scatter in the size of the larger aggregates.

holes, which cannot combine to form triplets. The polaron signal from PPE is likely red shifted from that of PPE^+ for several reasons. First, the π-overlap in the uncharged polymer may allow the polarons to migrate to lower energy sites. Next, if the charged polymer is assembled into a cylindrical micellar type structure, then it may have less opportunity to twist or kink than the uncharged polymer, thus preventing the formation of trap sites. Finally, the nearby cationic trimethylammonium group could destabilize the *p*-polaron, raising its energy with respect to the polaron on the uncharged PPE.

Dynamic light scattering (DLS) data, presented in Figures 7 and 8, shows the approximate sizes of the polymer aggregates in solution. It is important to note, however, that there can be large systematic errors in these values because the instrument relies on the calculation of the diffusion constant of a spherical particle based on an autocorrelation function.[37] The measured size therefore corresponds to spherical particles with the same diffusion constant as the polymer micelles in solution. In addition, the measurement is highly sensitive to the presence of impurities in the solution, necessitating scrupulous cleaning of glassware and solvents. Even so, it is difficult to eliminate

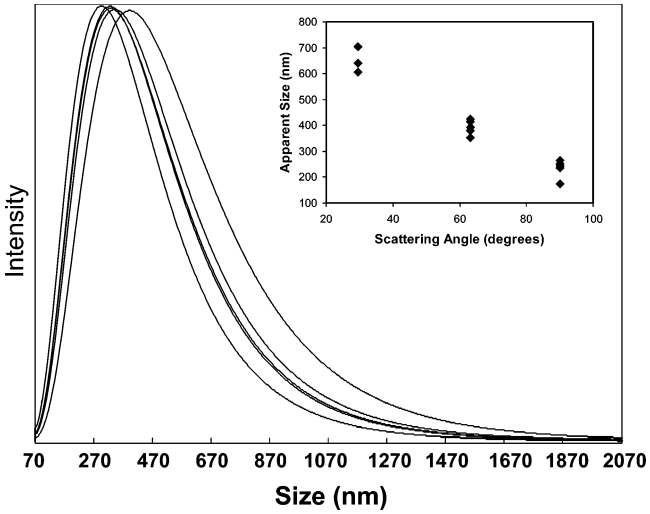

Figure 8. Unimodal light scattering data for PPE^+ collected at 60° showing reproducibility and an average size ~350 nm. Angle-dependent data (inset) shows a decrease in apparent size with increasing angle, consistent with DLS models for semiflexible wormlike micelles with fairly long persistence lengths.

all impurities, and the presence of a single unwanted particle can significantly affect the autocorrelation function on any particular trial. Therefore, it is necessary to perform multiple runs to build a statistical database, enabling the identification and rejection of outlying data points. Because of these difficulties, the size estimates obtained from DLS are not exact, but general trends can still be identified to corroborate the structural analysis from the photophysics data.

DLS data for the uncharged PPE are shown in Figure 7. At low concentrations, DLS should show smaller particles in solution, since the uncharged PPE chains should be individually solvated. However, the particle size analyzer employed in these experiments requires a relatively high concentration to maintain a high enough scattering intensity to collect reproducible results. Therefore, the data in Figures 7 and 8 were taken on PPE and PPE^+ solutions with concentrations of 0.2 mg/mL, which provided sufficient scattering intensity for the particle size analyzer to collect reproducible data. At similar concentrations (0.1 mg/mL), PPE should form aggregates as suggested by the UV−vis absorption and fluorescence data in Figures 1−3. According to the DLS data in Figure 7, it does form large aggregates with average size ~600 nm. Multimodal analysis of the data, however, did yield intensity from small (~10 nm) particles as well, indicating that there are still some nonaggregated polymer chains in solution, in agreement with the photophysics. These particles usually account for a high percentage of the number of particles in solution but for only a small amount of the total intensity, because the larger particles have much greater scattering length densities, dominating the DLS signal even though there are not as many in solution. This explains why there is no observable λ^{-4} scattering background in the optical absorption spectrum (Figure 1), as one might expect for a solution of particles with sizes in the visible range.

Figure 8 shows the unimodal size distribution for a sample of PPE^+ in ethanol collected at 60° off the excitation direction. The peak at ~350 nm again indicates that the polymer chains are aggregated. While any one set of data like that shown in Figure 8 cannot provide information about the shape of the species diffusing in solution, we have used a variety of methods to help suggest that the diffusing species are in fact the cylindrical micelles postulated throughout the paper. In the first place, the raw autocorrelation functions for both PPE and PPE^+ at a variety of angles were independently fit using both the simple sphere model described above and a rigid rod model.[38] While the PPE data could be well fit at all angles using the sphere model, the PPE^+ curves were not well fit by the sphere models, particularly at the highest angles (90°). This is suggestive of an anisotropic aggregate shape and the appearance of internal degrees of freedom in the diffusion such as rotations, which should be most evident at 90°.[38] The PPE^+ data also could not be well fit with a rigid rod model.[39] Moreover, the aggregate lengths needed to match the fundamental decay times observed in the data produced micelles with lengths on the order of micrometers when the diameter was fixed at a reasonable value based on molecular considerations.[40] Since the length of an individual chain is only about 75 nm,[40] the data suggests that the aggregates are significantly longer than a single polymer chain, implying that supramolecular assembly can produce aggregates with many parallel changes that could facilitate long-range conduction in these self-organized polymers.

The poor quality of the rigid rod fits, however, suggests that despite the fairly rigid molecular nature of the PPE chains and the added stiffness that comes from a self-organized cylindrical structure, the species found in solution cannot be well modeled as rigid rods. This is quite reasonable as it is unlikely that any solution-phase micelles could remain truly rigid on the scale of micrometers. The more likely scenario is what is often described as wormlike micelles, which lie between flexible chains and rigid rods in terms of stiffness.[41] In this case, the persistence length of the micelle (l_p) is smaller than the contour length of the micelle (L_c), but L_c/l_p is not $\gg 1$. In this situation, the DLS autocorrelation functions cannot be cleanly separated into translational and rotational components, as in the rigid rod case.[38] Instead, the data can be fit to produce only an average radius of gyration, as is the case with the data shown in Figure 8. When the data is collected at many angles, however, a decrease in apparent size is observed.[41] By analogy with the rigid rod case, this is because translational modes dominate at low scattering vectors, while internal degrees of freedom (bends and stretches for the wormlike micelle, rather than the rotations used for the rigid rod) are more important at higher scattering vectors.[41] The trend is clearly seen in our data (Figure 8, inset), where the apparent size as determined by DLS steadily decreases as a function of increasing collection angle. This trend is not observed for the uncharged PPE. Moreover, calculations show that this trend of decreasing apparent size as a function of increasing scattering vector is very robust to polydispersity,[41] something that is important for our materials which are likely to have a single micelle diameter but a broad range of micelle lengths. Based on this combination of results, we believe that the DLS data provides good structural conformation that the PPE^+ aggregate species in solution are, in fact, wormlike cylindrical micelles.

Conclusions

We have synthesized two facially amphiphilic poly(phenylene ethynylene)s and investigated their solution-phase assembly and optical properties. For the uncharged PPE, the degree of aggregation can be controlled by varying the concentration. By contrast, PPE^+ always aggregates in solution, as evidenced by planarization of the phenyl rings in the polymer chains and the accompanying red-shifted bands in the absorption and emission spectra. However, electrostatic repulsion between ammonium groups on the side chains of PPE^+ apparently forces neighboring chains too far apart for effective π-stacking, as evidenced by the lack of polaron or triplet production in photoinduced

absorption. This unique combination of planar yet weakly interacting PPE chains appears to arise from the formation of cylindrical micelles, which in turn arises from the amphiphilic nature of the PPE^+. DLS data further support this aggregation model and suggest that the solution-phase aggregates are semiflexible wormlike micelles.

PPE has great potential for use in optoelectonic materials because of its optical band gap and robust nature, even under ambient conditions. Geometrical confinement of the polymers has the potential to enhance a variety of their properties. One way to accomplish this is to incorporate polymers within the pores of mesoporous inorganic host materials. Our group and others have worked to confine conjugated polymers within nanostructured framework hosts to enhance optoelectronic[32,42−44] and mechanical properties,[45] to improve environmental stability,[46] and to achieve directed energy[47,48] or electron[49,50] transfer for use in nanostructured electronic devices. Semiconducting polymers such as polydiacetylene[51] and poly(phenylene butadiynylene)[52] have also been incorporated into mesoporous silica. Moreover, when the hosts are macroscopically oriented, this type of polymer incorporation can produce long-range alignment of polymer chains.[46,53]

Extending these concepts to the PPE system, interesting electronic materials could also be made by inserting PPE into an ordered mesoporous structure. This could allow the polymers to make elongated, wirelike domains with a more regular geometry than those likely to form in solution. The linear chain structure of PPE makes it behave essentially as a rigid rod even without being confined to a one-dimensional environment but incorporating it into a mesoporous host could make the composite mechanically more robust and increase the overall length of the linear domains. The amphiphilic nature of the side chains on each repeat unit gives PPE^+ a surfactant-like structure, making it an ideal candidate as the structure directing agent for the *direct* synthesis of a nanostructured electronic composite material. Using our experience with surfactant templated nanostructured oxides, we have thus investigated PPE^+ as the template to direct the assembly of mesostructured silica, which is discussed in another communication.[54] This method employs a facile, one-step synthesis of the functional composite material, giving it a significant synthetic advantage over other methods, such as infiltration of functionalized porous materials and in-situ polymerization. The optical properties of PPE, combined with its tendency to self-assemble, make it a promising system for functional optoelectonic nanostructures.

Acknowledgment. This work was supported by the Office of Naval Research (N00014-99-1-0568 (S.H.T) and N00014-04-1-0410 (S.H.T and Y.R)). Additional support was provided by NSF Grant CHE-0527015 (S.H.T. and Y.R.), by NSF Grants CHE-0080942 (Y.R.), CHE-9974928 (NMR), and DMR-0114002 (fluorometry), and by ACS-PRF Grant 39164-AC5M (Y.R.).

Supporting Information Available: Characterization of synthetic intermediates. This material is available free of charge via the Internet at http://pubs.acs.org.

References and Notes

(1) Friend, R. H.; Gymer, R. W.; Holmes, A. B.; Burroughes, J. H.; Marks, R. N.; Taliani, C.; Bradley, D. D. C.; Dos Santos, D. A.; Brédas, J. L.; Lögdlund, M.; Salaneck, W. R. *Nature* **1999**, *397*, 121.

(2) Zhou, Q.; Swager, T. M. *J. Am. Chem. Soc.* **1995**, *117*, 7017.

(3) Kim, J.; Levitsky, I. A.; McQuade, D. T.; Swager, T. M. *J. Am. Chem. Soc.* **2002**, *124*, 7710.

(4) Lovinger, A. J.; Rothberg, L. J. *J. Mater. Res.* **1996**, *11*, 1581.

(5) Dimitrakopoulos, C. D.; Malenfant, P. R. L. *Adv. Mater.* **2002**, *14*, 99.

(6) Burroughes, J. H.; Bradley, D. D. C.; Brown, A. R.; Marks, R. N.; Mackay, K.; Friend, R. H.; Burns, P. L.; Holmes, A. B. *Nature* **1990**, *347*, 539.

(7) Gustaffson, G.; Cao, Y.; Treacy, G. M.; Klavetter, F.; Colinari, N.; Heeger, A. J. *Nature* **1992**, *357*, 477.

(8) Hide, F.; Schwartz, B. J.; DiazGarcia, M. A.; Heeger, A. J. *Chem. Phys. Lett.* **1996**, *256*, 424.

(9) Scherf, U.; Riechel, S.; Lemmer, U.; Mahrt, R. F. *Curr. Opin. Solid State Mater.* **2001**, *5*, 143.

(10) Granstrom, M.; Petritsch, K.; Arias, A. C.; Lux, A.; Andersson, M. R.; Friend, R. H. *Nature* **1998**, *395*, 257.

(11) Brabec, C. J.; Sariciftci, N. S.; Hummelen, J. C. *Adv. Funct. Mater.* **2001**, *11*, 15.

(12) Yang, J. S.; Swager, T. M. *J. Am. Chem. Soc.* **1998**, *120*, 11864.

(13) Bumm, L. A.; Arnold, J. J.; Cygan, M. T.; Dunbar, T. D.; Burgin, T. P.; Jones, L.; Allara, D. L.; Tour, J. M.; Weiss, P. S. *Science* **1996**, *271*, 1705.

(14) Montali, A.; Bastiaansen, G.; Smith, P.; Weder, C. *Nature* **1998**, *392*, 261.

(15) Halkyard, C. E.; Rampey, M. E.; Kloppenburg, L.; Studer-Martinez, S. L.; Bunz, U. H. F. *Macromolecules* **1998**, *31*, 8655.

(16) Kim, J.; Swager, T. M. *Science* **2001**, *411*, 1030.

(17) Okuyama, K.; Hasegawa, T.; Ito, M.; Mikami, N. *J. Phys. Chem.* **1984**, *88*, 1711.

(18) Miteva, T.; Palmer, L.; Kloppenburg, L.; Neher, D.; Bunz, U. H. F. *Macromolecules* **2000**, *33*, 652.

(19) Kim, J.; Levitsky, I. A.; McQuade, D. T.; Swager, T. M. *J. Am. Chem. Soc.* **2002**, *124*, 7710.

(20) Breitenkamp, R.; Tew, G. N. *Macromolecules* **2004**, *37*, 1163.

(21) Arnt, L.; Tew, G. N. *J. Am. Chem. Soc.* **2002**, *124*, 7664.

(22) Tan, C.; Pinto, M. R.; Schanze, K. S. *Chem. Commun.*, **2002**, 446.

(23) Pinto, M. R.; Schanze, K. S. *Synthesis*, **2002**, *9*, 1293.

(24) Nguyen, T.-Q.; Schwartz, B. J. *J. Chem. Phys.* **2002**, *116*, 8198.

(25) See Supporting Information for spectroscopic data on all synthesized compounds. For more information on the synthesis of these polymers, see: Shen, C. K.-F. Ph.D. Thesis, University of California, Los Angeles, Los Angeles, CA, 2004.

(26) Peng, Z. H.; Gharavi, A. R.; Yu, L. P. *J. Am. Chem. Soc.* **1997**, *119*, 4622−4632.

(27) Sonogashira, K.; Tohda, Y.; Hagihara, N. *Tetrahedron Lett.* **1975**, 4467−4468.

(28) Private discussion during the 225th ACS meeting, New Orleans, LA, 2003.

(29) Fiesel, R.; Scherf, U. *Macromol. Rapid Commun.* **1998**, *19*, 427.

(30) Motamedi, F.; Ihn, K. J.; Ni, Z.; Srdanov, G.; Wudl, F. *Polymer* **1992**, *33*, 1102.

(31) Frankevich, E. L.; Lymarev, A. A.; Sokolik, I.; Karasz, F. E.; Blumstengel, S.; Baughman, R. H.; Hörhold, H. H. *Phys Rev B.* **1992**, *46*, 9320.

(32) Cadby, A. J.; Tolbert, S. H. *J. Phys. Chem. B* **2005**, *109*, 17879.

(33) Wei, X.; Vardeny, Z. V.; Sariciftci, N. S.; Heeger, A. J. *Phys. Rev. B* **1996**, *53*, 2187.

(34) Christiaans, M. P. T.; Van Hal, P. A.; Janssen, R. A. J.; Wienk, M. M.; Kroon, J. M. *Synth. Met.* **1999**, *101*, 265.

(35) Jiang, X. M.; Wu, C. C.; Wohlgenannt, M.; Huang, W. Y.; Kwei, T. K.; Okamoto, Y.; Vardeny, Z. V. *Physica B*, **2003**, *338*, 235.

(36) Janssen, R. A. J.; Sariciftci, N. S.; Pakbaz, J.; McNamara, J. J.; Schricker, S.; Heeger, A. J.; Wudl, F. *Synth. Met.* **1995**, *69*, 441.

(37) Schmitz, K. S. *An Introduction to Dynamic Light Scattering by Macromolecules*; Academic Press: Boston, MA, 1990.

(38) Berne, B. J.; Pecora, R. *Dynamic Light Scattering: With Applications to Chemistry, Biology, and Physics*; Wiley: New York, 1976.

(39) Santos, N. C.; Castanho, M. A. R. B. *Biophys. J.* **1996**, 1641.

(40) Energy minimization was performed on a PPE trimer using CambridgeSoft ChemBats3D Ultra 6.0 MM2 Minimize Energy to minimum the RMS gradient of 0.01. The distance between the ends of the side chains on a PPE monomer of 1.7 nm was used to estimate a micelle diameter of 4−5 nm. The length of the trimer was also extrapolated to the length of the polymer based on the average molecular weight from GPC.

(41) von Berlepsch, H.; Harnau, L.; Reineker. P. *J. Phys. Chem. B* **1998**, *102*, 7518.

(42) Nguyen, T.-Q.; Wu, J.; Tolbert, S. H.; Schwartz, B. J. *Adv. Mater.* **2001**, *13*, 609.

(43) Tolbert, S. H.; Wu, J.; Gross, A. F.; Nguyen, T.-Q.; Schwartz, B. J. *Microporous Mesoporous Mater.* **2001**, *44*−*45*, 445.

(44) Park, J. H.; Kim, S.; Kim, Y. C.; Park, O. O. *Nanotechnology* **2005**, *16*, 1793.

(45) Kirsch, B. L.; Chen, X.; Richman, E. K.; Gupta, V.; Tolbert, S. H. *Adv. Funct. Mater.* **2005**, *15*, 1319.

(46) Wu, J. J.; Gross, A. F.; Tolbert, S. H. *J. Phys. Chem. B* **1999**, *103*, 2374−2384.
(47) Nguyen, T.; Wu, J.; Doan, V.; Schwartz, B. J.; Tolbert, S. H. *Science* **2000**, *288*, 652.
(48) Schwartz, B. J.; Nguyen, T.-Q.; Wu, J.; Tolbert, S. H. *Synth. Met.* **2001**, *116*, 35.
(49) Coakley, K. M.; Liu, Y. X.; McGehee**,** M. D.; Frindell, K. L.; Stucky, G. D. *Adv. Funct. Mater.* **2003**, *13*, 301.
(50) Coakley, K. M.; McGehee, M. D. *Appl. Phys. Lett.* **2003**, *83*, 3380.
(51) Lu, Y.; Yang, Y.; Sellinger, A.; Lu, M.; Huang, J.; Fan, H.; Haddad, R.; Lopez, G.; Burns, A. R.; Sasaki, D. Y.; Shelnutt, J.; Brinker, C. J. *Nature* **2001**, *410*, 913.
(52) Lin, V. S.-Y.; Radu, D. R.; Han, M.-K.; Deng, W.; Kuroki, S.; Shanks, B. H.; Pruski, M. *J. Am. Chem. Soc.* **2002**, *124*, 9040.
(53) Molenkamp, W. C.; Watanabe, M.; Miyata, H.; Tolbert, S. H. *J. Am. Chem. Soc.* **2004**, *126*, 4476−4477.
(54) Clark, A. P.-Z.; Shen, K.-F.; Rubin, Y. F.; Tolbert, S. H. *Nano Lett.* **2005**, *5*, 1647.